



## Torque Density Improvement in Transverse Flux Machine using Disc Rotor

---

Balaganesh Boomiraja and Ragavan Kanagaraj

EasyChair preprints are intended for rapid dissemination of research results and are integrated with the rest of EasyChair.

November 19, 2019

# Torque Density Improvement in Transverse Flux Machine using Disc Rotor

Balaganesh Boomiraja, *Student Member IEEE*, and Ragavan Kanagaraj, *Member IEEE*  
*Electrical Engineering, Indian Institute of Technology Gandhinagar*

Gujarat, India - 382355

Email: balaganesh.b@iitgn.ac.in, ragavan@iitgn.ac.in

**Abstract**—Transverse flux machines are usually designed with either cylindrical rotor or disc rotor structure. In this paper, a disc rotor topology with single layer of permanent magnets per phase is proposed to improve the torque density. Unlike conventional transverse flux machine, the stator construction is simplified by joining c-cores of all phase stacks together in the proposed design. Analytical equations are derived for calculating the electromagnetic torque, magnetizing inductance, and leakage inductance. The disc rotor transverse flux machine is compared with an equivalent cylindrical rotor transverse flux machine using finite element analysis simulation. It is found that the transverse flux machine with disc rotor has higher torque density than that of cylindrical rotor topology.

**Index Terms**—Transverse flux machine, permanent magnet, disc rotor, cylindrical rotor, FEA

## I. INTRODUCTION

Electrical machines are classified as longitudinal and transverse based on the orientation of flux plane with direction of rotor motion. The orientation of flux plane with respect to the direction of motion is parallel for longitudinal flux machine (LFM) and perpendicular for transverse flux machine (TFM). Transverse Flux concept was introduced by Laithwaite et al. in 1971 [1]. Transverse flux machine offers high torque density when it is designed with large number of poles [2]–[4]. However, it operates at low power factor [3]–[9] which leads to poor utilization of the inverter. Leakage reactance is the main cause for low power factor operation of TFM [4], [6]. In [9], the dependency of the torque and power factor on the number of poles for a given diameter of TFM is studied.

In [10], a magnetic shunt (iron bar) is used to reduce the pole leakage flux and to increase useful flux. This topology improved the power factor and efficiency of TFM. However, the magnetic shunt complicates the manufacturing process and this topology is preferred for large size machines [11]. A modular permanent magnet TFM with disc shape rotor is proposed in [12]. Therein the power factor value is reported as 0.89 at 4 A/mm<sup>2</sup> current density. In this design, the permanent magnets are arranged in two layers. As a result, each stator phase is made with two stacks of c-cores and manufacturing becomes complicated.

Herein, a disc rotor topology of transverse flux permanent magnet machine is proposed to improve the performance and to simplify the manufacturing process. Unlike the conventional TFM designs, poly-phase stator stacks are joined together

which simplifies the stator construction and reduces the machine volume. Also, the rotor has one layer of permanent magnets per phase stack. As the rotor disc is made of non-magnetic material, it is safe and easy to embed permanent magnet in it. Analytical equations of torque and phase winding inductance are derived for disc rotor topology.

## II. STRUCTURE AND WORKING PRINCIPLE

The structural difference between the cylindrical rotor and disc rotor TFM is shown in Fig. 1. A non-magnetic stator frame which holds the stator c-cores together is not shown in this figure for better visibility. The cylindrical rotor design has radial air-gap flux. The stator is made of three individual phase stacks which are stacked with gap in between them to reduce phase-phase pole leakage flux at the air-gap. Each stator phase stack has a ring-shaped coil with  $Z$  number of turns. In this configuration, permanent magnets are arranged in two layers for each phase stack as shown in Fig. 1a.

The disc rotor design has air-gap flux in the axial direction. In this topology, the stator phases are stacked together without gap between phase stacks as shown in Fig. 1b. Each phase stack has a ring-shaped coil and a non-magnetic rotor rim in which permanent magnets are embedded. Three such rotor rims with 120° electrical degree displacement between them are shown in Fig. 1b. These rims can be joined together by an outer rotor cylinder which is not shown in the figure. If a single-phase stack has  $p$  number of c-cores, the disc rotor topology needs  $2p$  number of magnets whereas cylindrical rotor design requires  $4p$  magnets. Manufacturing of disc rotor is simpler than that of cylindrical rotor. However, alignment of stator and rotor will be a challenge in disc rotor design. A c-core of disc rotor TFM is shown in Fig. 2. The stator pole shoe area  $A_{sp}$  is higher than the cross-section area  $A_{sy}$  at middle of c-core. This increases flux density in the c-core and hence utilization of the core material gets improved.

The axial view of disc rotor design is shown in Fig. 3 and the parameters mentioned are as follows.  $D_o$  is stator outer diameter,  $D_{ag}$  is average air-gap diameter,  $D_c$  is average coil diameter,  $\gamma_s$  is stator pole pitch,  $\gamma_r$  is rotor pole pitch,  $\beta_s$  is stator pole arc length,  $\beta_r$  is rotor pole arc length, and  $h_1$  is pole shoe length in radial direction. In Fig. 3, south pole of PM is aligned with the top of c-core. As the rotor revolves, north pole will align with c-core and the flux in the c-core reverses. With the continuous rotation, magnetic field in the c-core becomes

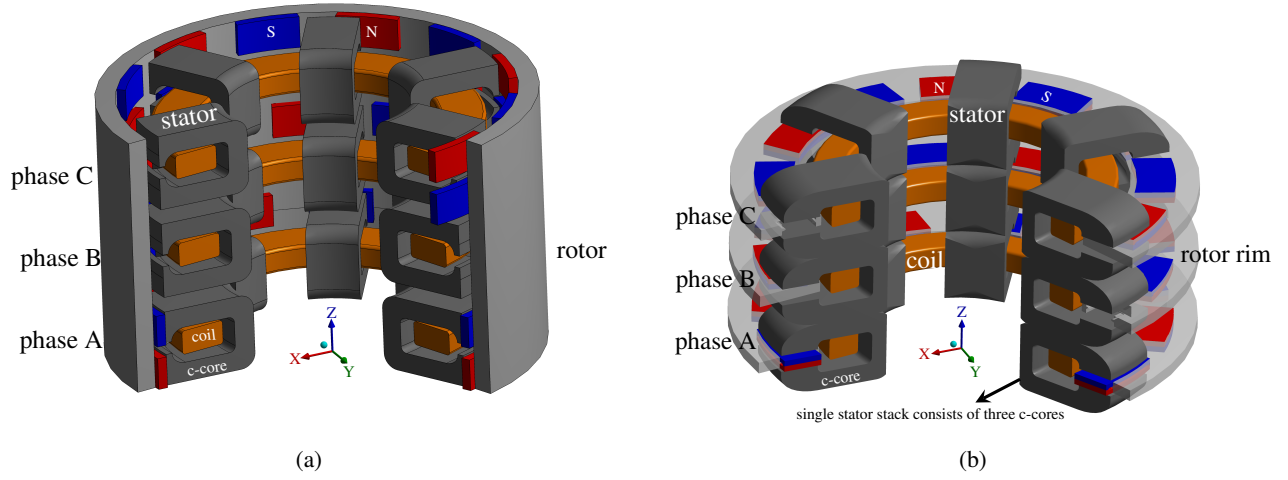


Fig. 1: Cut-section view of TFM (a) cylindrical rotor; and (b) disc rotor

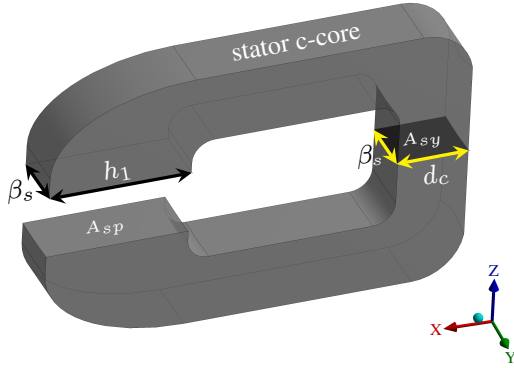


Fig. 2: Cut-section view of single c-core

pulsating. Due to this pulsating magnetic field, emf is induced in the phase winding. Maximum electromagnetic torque for the given current can be developed by making the phase current in-phase with the induced emf.

### III. ELECTROMAGNETIC TORQUE

In this section, torque developed by the disc rotor TFM is derived in terms of electrical and magnetic loading. Consider the axial cross-section view shown in Fig. 3. The electric loading  $A$  is given by

$$A = \frac{IZ}{\pi D_{ag}} \quad (1)$$

where,  $I$  is rated rms current of the conductor, and  $Z$  is total number of conductors in phase winding. Net flux  $\Phi_m$  encircling the phase winding (when rotor pole is aligned with the stator c-core) is given by

$$\Phi_m = p\beta_s h_1 B_{pm} K_s K_{pl} \quad (2)$$

where,  $h_1$  is stator pole face length,  $\beta_s = \frac{\pi D_{ag}}{2p} \frac{\alpha_s}{180}$  is stator pole arc length,  $\alpha_s$  is stator pole arc,  $B_{pm} = B_r \frac{h_m}{h_m + l_{ag}}$  is

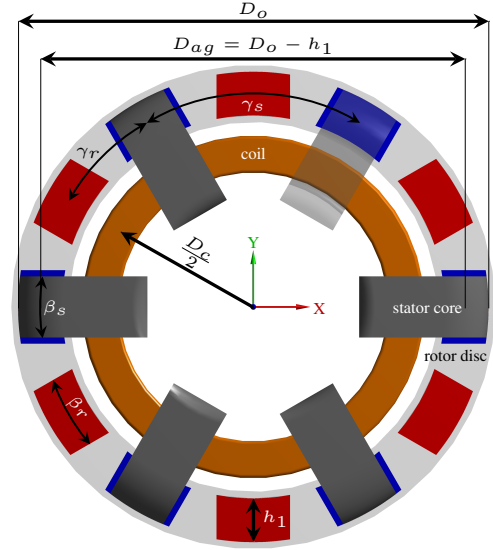


Fig. 3: Axial view of one phase stack of disc rotor TFM

the ideal flux density in air-gap [13],  $h_m$  is permanent magnet thickness,  $l_{ag}$  is air-gap thickness,  $K_s$  is stacking factor, and  $K_{pl}$  is pole leakage flux coefficient. As rotor rotates, the flux through c-core is pulsating. The fundamental of phase flux  $\phi_1(t)$  is given by

$$\phi_1(t) = \frac{\pi D_{ag}}{2} \frac{\alpha_s}{180} h_1 B_{pm} K_s K_{pl} \cos(p\omega_r t) \quad (3)$$

where,  $\omega_r$  is rotor speed, and  $t$  is time. By Faraday's law of induction, electromotive force (EMF) induced in the phase winding is given by

$$e_{ph} = -Z \frac{d\phi_1(t)}{dt} = p\omega_r Z \frac{\pi D_{ag}}{2} \frac{\alpha_s}{180} h_1 B_{pm} K_s K_{pl} \sin(p\omega_r t) \quad (4)$$

Net electromagnetic torque ( $T_{em}$ ) developed by three phases is given by

$$T_{em} = \frac{3EI\cos(\Psi)}{\omega_r} \quad (5)$$

where  $E$  is rms value of induced emf and  $\Psi$  is phase difference between current and EMF. By substituting (1) and (4) in (5)

$$T_{em} = p \frac{3\pi^2}{2\sqrt{2}} \frac{\alpha_s}{180} h_1 D_{ag}^2 AB_{pm} K_s K_{pl} \cos(\Psi) \quad (6)$$

Equation (6) shows that the torque developed in disc rotor TFM is directly proportional to electrical loading, magnetic loading and number of c-core. By increasing the number of c-cores torque can be improved. But with large number of poles, the pole leakage also increases. Pole leakage flux coefficient may be the limiting factor for the number of c-cores.

#### IV. PHASE WINDING INDUCTANCE

The phase winding inductance consist of magnetizing and leakage inductance. Power factor of TFM is mainly depend on the phase inductance value. In this section, derivation of magnetizing and leakage inductance is presented. The leakage inductance includes slot leakage, end winding leakage, and fringing leakage effects. Geometric parameters of c-core shown in Fig. 4 are used in the derivation.

##### A. Magnetizing Inductance

Inductance corresponding to the production of useful pulsating magnetic field in the air-gap is known as magnetizing inductance. It is calculated with the following assumptions.

- The core material is operating in linear region.
- Flux density in the c-core is uniform.

Consider the cut-section view of c-core shown in Fig. 2, and cross-section view shown in Fig. 4. The magnetizing inductance is given by

$$L_m = p\mu Z^2 \left[ \frac{A_{sp}}{\mu_r b_1} + \frac{A_{sy}}{l_c} + \frac{A_{sp}}{2l_f} \right] \quad (7)$$

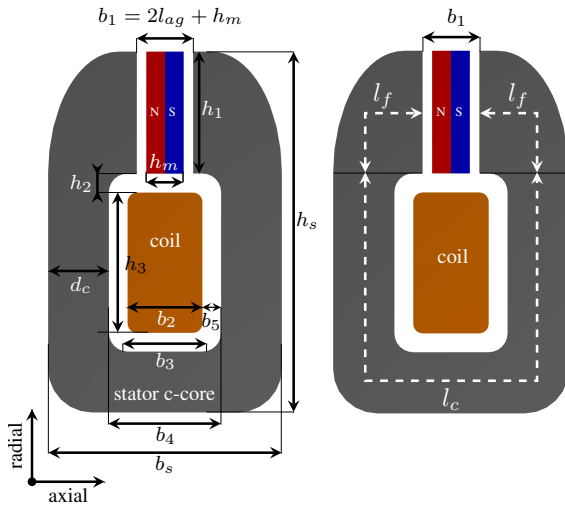


Fig. 4: Cross-section view of c-core

where,  $A_{sp}$  is stator pole face area,  $b_1$  is total air-gap length,  $l_f$  is length of c-core at front portion,  $A_{sy}$  is c-core cross section area, and  $l_c$  is c-core length.

##### B. Leakage Inductance

1) *Slot Leakage Inductance*: The flux lines passing through the slot at the heights  $h_2$  and  $h_3$  in axial direction (refer Fig. 4) which are not reaching the air-gap but links the coil. This flux is known as slot leakage flux and the corresponding inductance is slot leakage inductance  $L_u$ . It is assumed that the core has relatively very high permeability than the material inside the slot. The slot leakage inductance is calculated as given in [14] for the slot shown in Fig. 4

$$L_u = p\mu_0 \beta_s Z^2 \left[ \frac{h_3}{3b_4} + \frac{h_2}{(b_4 - b_3)} \ln \left( \frac{b_4}{b_3} \right) \right] \quad (8)$$

2) *End winding Leakage Inductance*: Some portion of the phase coil are not covered by the stator c-core (refer Fig. 3), which are producing flux that is not useful for the energy conversion. The inductance corresponding to this is known as end winding inductance  $L_w$  of TFM. This inductance can be calculated as the parallel conductors suspended in air [4]. As per the dimensions given in the Fig. 3, the end-winding leakage is

$$L_w = \frac{p\mu_0}{2\pi} \beta_c Z^2 \left[ \frac{1}{4} + \ln \left( \frac{D_c}{b_2/2} \right) \right] \quad (9)$$

The end winding leakage flux links with other phase coils and contributing for mutual inductance between phases. The corresponding mutual inductances are

$$L_{ABw} = L_{BCw} = \frac{p\mu_0}{2\pi} \beta_c Z^2 \left[ \frac{1}{4} + \ln \left( \frac{D_c}{b_s} \right) \right] \quad (10)$$

$$L_{ACw} = \frac{p\mu_0}{2\pi} \beta_c Z^2 \left[ \frac{1}{4} + \ln \left( \frac{D_c}{2b_s} \right) \right] \quad (11)$$

3) *Fringing flux Inductance*: A part of the magnetic flux produced from c-core is fringing in the air (not passing through PM). The inductance corresponds to flux fringing is given by

$$L_{fringe} = p\mu Z^2 \left[ \frac{A_{sp}}{\mu_r b_1} + \frac{A_{sy}}{l_c} + \frac{A_{sp}}{2l_f} \right] k_{area} \quad (12)$$

where  $k_{area}$  is flux fringing area coefficient. The fringing flux also links with other phase coils. The mutual inductance between phases A and B due to fringing flux is given by

$$L_{fringeAB} = k_{AB} \sqrt{L_{fringeA} L_{fringeB}} \quad (13)$$

where  $k_{AB}$  is coefficient of coupling. The value of  $k_{area}$  and  $k_{AB}$  are need to be found from finite element analysis (FEA) simulation.

## V. FINITE ELEMENT ANALYSIS SIMULATION

Electromagnetic analysis of cylindrical rotor and disc rotor TFM is done using finite element analysis (FEA). Also, magnetizing inductance and leakage inductance of disc rotor design are calculated using FEA. Flux plane of TFM is normal to the direction of rotor motion. Due to this, 3D-FEA package (Ansys-maxwell) is used to solve. The complete structure of TFM need not be modelled to get the machine characteristics. One pole pair model of cylindrical rotor (M1) and disc rotor (M2) shown in Fig. 5 are solved with symmetry multiplier of  $p$  to get the performance characteristics of one phase stack. The symmetry of machine is utilized to reduce simulation time.

Design specifications of cylindrical rotor and disc rotor TFM are given in Table I. A 0.2 mm thick silicon steel (130Y320) is assigned as material for stator and rotor core. C-cores are laminated in azimuthal direction with 0.85 stacking factor. The permanent magnet residual flux density is assumed as 1.2 T. Number of turns in the coil is considered as 24. With this design parameter machines are modelled and finite element analysis is done.

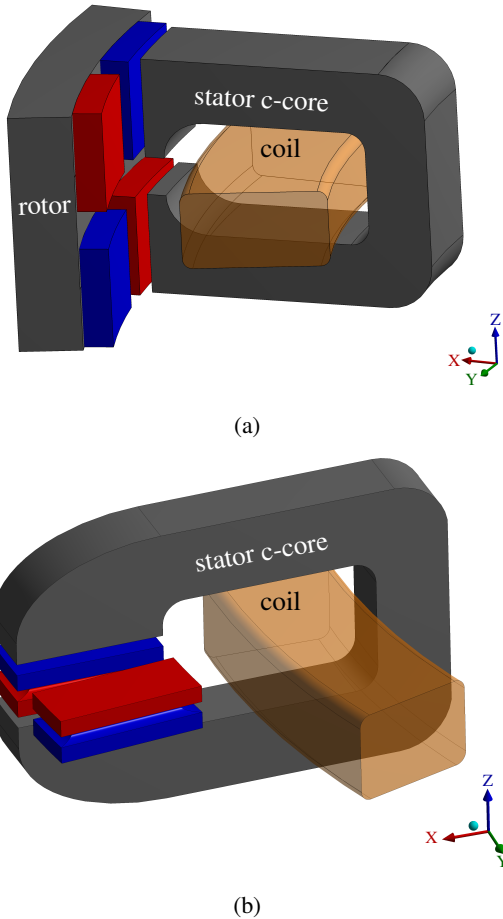


Fig. 5: One pole pair of TFM (a) cylinder rotor - M1; and (b) disc rotor - M2

TABLE I: Specifications of TFM

Parameter	Symbol	M1	M2
Rotor outer diameter (mm)	$D_o$	200	200
Stator inner diameter (mm)	$D_i$	119	119
Air-gap diameter (mm)	$D_{ag}$	180	187
Coil diameter (mm)	$D_c$	151	151
Stack length (mm)	$b_s$	25	25
PM thickness (mm)	$h_m$	3	6
Number of c-cores	$p$	18	18
Stator pole arc (mm)	$\beta_s$	9.9	9.9
Rotor pole arc (mm)	$\beta_r$	12.1	12.1
c-core depth (mm)	$d_c$	6.5	6.5
Slot height (mm)	$h_{sl}$	21	21
Slot width (mm)	$b_A$	12	12
Slot fill factor		0.48	0.48
Net core weight (kg)	$m_{core}$	4.52	2.45
Net PM weight (kg)	$m_{mag}$	0.62	0.73
Net coil weight (kg)	$m_{coil}$	0.91	0.91

### A. Without armature excitation

The rotor of TFM shown in Fig. 5 are rotated at rated speed (3200 rpm) with armature winding kept open. Obtained induced emf and cogging torque are plotted in Fig. 6. The flux linkage, induced voltage and cogging torque of disc rotor machine are better than cylindrical rotor machine. In cylindrical rotor, the number of magnets is twice than that of disc rotor for same pole design; as a result pole flux leakage is more in cylindrical rotor design. The induced voltage of disc rotor TFM calculated from analytical and FEA methods are 106 V and 102.2 V respectively. In analytical method, saturation effect is neglected which causes 3.7% error in calculation.

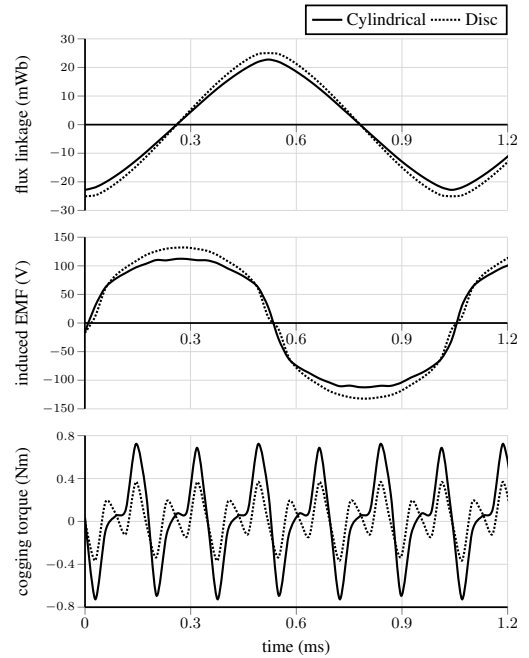


Fig. 6: FEA results of cylindrical rotor and disc rotor TFM at no-load

### B. With armature excitation

FEA models shown in Fig. 5 is solved with armature excitation. The sinusoidal current is injected in-phase with emf to develop maximum torque per ampere. Net torque and power factor of TFM are calculated by post-processing the FEA results. Torque produced by disc rotor (M2) is higher than that of cylindrical rotor (M1). Variation of torque and power factor with armature current is plotted in Fig. 7. The active mass of disc rotor machine is 33% lower than that of cylindrical rotor machine. The torque density of M1 and M2 are 2.69 Nm/kg, and 4.38 Nm/kg respectively. The obtained machine rating of both machines are listed in Table II.

### C. Phase inductance

The phase inductance of disc rotor TFM is calculated using FEA. By default, FEA gives net inductance of phase winding. In this section, the magnetizing inductance and various leakage inductances are separately calculated using FEA. When calculating the magnetizing inductance, leakage inductance effect is nullified by using magnetic property of superconductor material to the leakage flux path.

1) *Magnetizing Inductance*: FEA model to find the magnetizing inductance of disc rotor TFM is shown in Fig. 8. Superconducting material is applied for the region (other than stator c-core, air-gap, and coil) in order to offer high value of reluctance to the leakage fluxes. In this simulation, only magnetizing flux will encircle the coil, and hence simulated inductance is equal to magnetizing inductance of TFM.

2) *Slot Leakage Inductance*: From the FEA simulation result of other inductances, slot leakage is calculated as  $L_u = L_{net} - L_m - L_w - L_{fringe}$ , where  $L_{net}$  is net inductance of the coil.

3) *End winding Leakage Inductance*: FEA model shown in Fig. 9 gives the end winding leakage and fringing flux in-

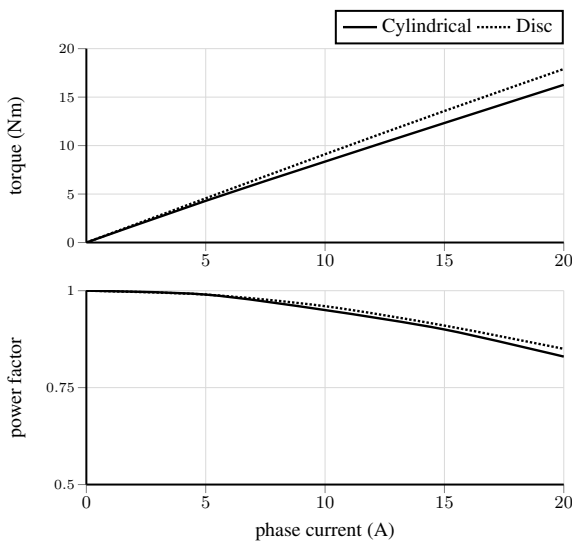


Fig. 7: Effect of armature current in cylindrical rotor and disc rotor TFM

TABLE II: Comparison of cylindrical rotor and disc rotor TFM

Parameter	M1	M2
Induced voltage (V)	90	102
Base speed (rpm)	3200	3200
Current (for 4 A/mm <sup>2</sup> ) (A)	20	20
Active mass (kg)	6.05	4.09
Torque (Nm)	16.27	17.9
Torque/mass (Nm/kg)	2.69	4.38
Power factor	0.83	0.85

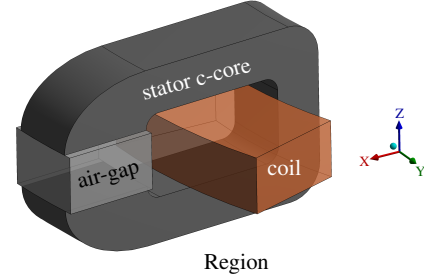


Fig. 8: FEA model to simulate magnetizing inductance

ductance. Superconducting material is assigned for the objects 1 and 2. This offers large reluctance to the magnetizing and slot leakage flux. The inductance calculated from simulation is combination of end winding leakage and fringing flux inductance. The fringing flux inductance is subtracted from this inductance to get end winding leakage inductance.

4) *Fringing flux Inductance*: FEA model to simulate fringing flux inductance is shown in Fig. 10. For the objects 1,2 and 3, superconducting material is applied. This provides large reluctance to magnetizing, slot leakage and end winding leakage fluxes.

Various inductances calculated using FEA and analytical expression are listed in Table III and Table IV respectively. Analytically determined inductance values are matching with the FEA results. The net leakage inductance is three times of magnetizing inductance. Fringing flux inductance is higher than other leakage inductances. High value of leakage inductance is the main cause for low power factor operation of TFM at high current densities (above 5 A/mm<sup>2</sup>).

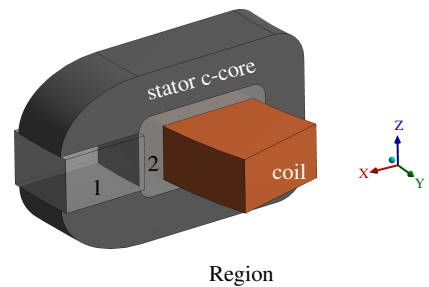


Fig. 9: FEA model to simulate end winding leakage and fringing flux inductance

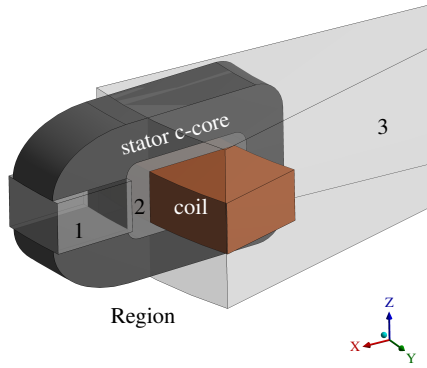


Fig. 10: FEA model to simulate fringing flux inductance

TABLE III: Winding inductance value of disc rotor TFM obtained from FEA

( $\mu\text{H}$ )	$L_A$	$L_B$	$L_C$	$L_{AB}$	$L_{BC}$	$L_{AC}$
$L_m$	146	146	146	0	0	0
$L_u$	51	52	50	0	0	0
$L_w$	71	71	71	34	34	28
$L_{fringe}$	330	376	330	108	107	50
$L_{net}$	598	643	597	142	141	78

TABLE IV: Analytically calculated inductance value of disc rotor TFM

( $\mu\text{H}$ )	$L_A$	$L_B$	$L_C$	$L_{AB}$	$L_{BC}$	$L_{AC}$
$L_m$	143	143	143	0	0	0
$L_u$	55	55	55	0	0	0
$L_w$	75	75	75	39	39	26
$L_{fringe}$	323	367	324	106	105	49
$L_{net}$	596	640	597	145	144	75

## VI. CONCLUSION

The performance of cylindrical rotor and proposed disc rotor TFM are compared using FEA. Torque density of the cylindrical rotor machine is 2.69 Nm/kg, and disc rotor machine is 4.38 Nm/kg. The higher torque density is due to reduced core weight in disc rotor design. The analytical expression for calculating torque and various inductance are derived for disc rotor TFM. There is good agreement between analytical and FEA results. Leakage inductance of disc rotor machine is three times of its magnetizing inductance. Though the manufacturing of rotor disc is relatively easy, alignment of stator and rotor will be a challenge in disc rotor design.

## REFERENCES

- [1] E. Laithwaite, J. Eastham, H. Bolton, and T. Fellows, "Linear motors with transverse flux," in *Proceedings of the Institution of Electrical Engineers*, vol. 118, pp. 1761–1767, 1971.
- [2] R. Kruse, G. Pfaff, and C. Pfeiffer, "Transverse flux reluctance motor for direct servodrives applications," in *IEEE Conf. Ind. Applicat. Soc. Annu. Meeting*, vol. 1, pp. 655–662, 1998.
- [3] G. Henneberger and M. Bork, "Development of a new transverse flux motor," in *IEE Colloq. New Topologies Permanent Magnet Machines*, pp. 1/1–1/6, Jan. 1997.
- [4] W. M. Arshad, T. Backstrom, and C. Sadarangani, "Analytical design and analysis procedure for a transverse flux machine," in *IEEE Int. Conf. Electric Machines and Drives*, pp. 115–121, Jun. 2001.
- [5] M. Harris, G. Pajooman, and S. A. Sharkh, "The problem of power factor in vrpm (transverse-flux) machines," in *IET Int. Conf. Elect. Machines and Drives*, pp. 386–390, Sep. 1997.
- [6] J. F. Gieras, "Performance characteristics of a transverse flux generator," in *IEEE Int. Conf. Electric Machines and Drives*, pp. 1293–1299, May 2005.
- [7] M. R. J. Dubois, *Optimized permanent magnet generator topologies for direct-drive wind turbines*. PhD thesis, Delft University, 2004.
- [8] C. Liu, J. Zhu, Y. Wang, G. Lei, and Y. Guo, "Design considerations of pm transverse flux machines with soft magnetic composite cores," *IEEE Trans. Appl. Supercond.*, vol. 26, pp. 1–5, Jun. 2016.
- [9] J. R. Anglada and S. M. Sharkh, "An insight into torque production and power factor in transverse-flux machines," *IEEE Trans. Ind. Applicat.*, vol. 53, pp. 1971–1977, May/Jun. 2017.
- [10] O. Dobzhanskyi, R. Gouws, and E. Amiri, "On the role of magnetic shunts for increasing performance of transverse flux machines," *IEEE Trans. Magn.*, vol. 53, pp. 1–8, Feb. 2017.
- [11] O. Dobzhanskyi, R. Gouws, and E. Amiri, "Analysis of pm transverse-flux outer rotor machines with different configuration," *IEEE Trans. on Ind. Applicat.*, vol. 53, pp. 4260–4268, Sep. 2017.
- [12] S. Hosseini, J. S. Moghani, N. F. Ershad, and B. B. Jensen, "Design, prototyping, and analysis of a novel modular permanent-magnet transverse flux disk generator," *IEEE Trans. Magn.*, vol. 47, pp. 772–780, Apr. 2011.
- [13] I. Boldea, J. Zhang, and S. A. Nasar, "Theoretical characterization of flux reversal machine in low-speed servo drives-the pole-pm configuration," *IEEE Trans. Ind. Applicat.*, vol. 38, pp. 1549–1557, Nov./Dec. 2002.
- [14] J. Pyrhonen, T. Jokinen, and V. Hrabovcova, *Design of rotating electrical machines*. John Wiley & Sons, 2013.